Available online at www.sciencedirect.com

ScienceDirect

Ceramics International 40 (2014) 13249–13256

CERAMICS INTERNATIONAL

www.elsevier.com/locate/ceramint

Structure and multiferroic properties of Sr substituted $Bi_{0.89-x}Sm_{0.11}Sr_xFe_{0.94}(Mn_{0.04}Cr_{0.02})O_3$ thin films

Wenlong Liu, Guoqiang Tan*, Xu Xue, Guohua Dong, Huijun Ren, Ao Xia

School of Materials Science and Engineering, Shaanxi University of Science & Technology, Xi'an 710021, China

Received 20 April 2014; received in revised form 8 May 2014; accepted 9 May 2014
Available online 16 May 2014

Abstract

Sr^{2+} substituted $Bi_{0.89-x}Sm_{0.11}Sr_xFe_{0.94}(Mn_{0.04}Cr_{0.02})O_3$ (BSSrFMC, $x=0.00$ 0.02, 0.04 and 0.06) thin films were prepared on FTO/glass (SnO_2:F) substrates by using a sol–gel method. The effects of Sr^{2+} substitution on the structure, leakage current, dielectric, ferroelectric and magnetic properties of BSSrFMC thin films have been investigated. X-ray diffraction (XRD), Rietveld refinement of XRD patterns and Raman spectroscopy results indicated two space groups (P4 and P422) to coexist in the tetragonal BSSrFMC thin film when $x=0.04$. Meanwhile, the lattice constant a was increased compared with that of the non-doped BSFMC thin film, which may result in an expanded unit cell. Highly enhanced multiferroic properties were observed in the BSSrFMC thin film with $x=0.04$, i.e., large remanent polarization ($2P_r=173.43$ μC/cm^2), and large saturated magnetization ($M_s=2.3$ emu/cm^3). Furthermore, a giant dielectric constant of 290 was observed in the $BSSr_xFMC$ ($x=0.04$) thin film at 1 kHz.

Keywords: A. Sol–gel processes; C. Ferroelectric properties; C. Magnetic properties; D. Ferrites

1. Introduction

As a multiferroic material, bismuth ferrite (BFO) is perhaps the only material which exhibits ferroelectric ($T_C=1103$ K) and G-type anti-ferromagnetic ($T_N=643$ K) properties simultaneously at room temperature [1–3]. In recent years, it has been widely studied due to fascinating fundamental physical properties and potential applications in the electronic information storage, spintronic devices and integrated microelectronic memory devices [4,5]. However, pure BFO thin film still shows high leakage currents, unsaturation P–E hysteresis loops and weak ferromagnetic properties due to the existence of oxygen vacancies and anti-ferromagnetic structures [6].

In order to reduce the leakage current and enhance the multiferroic properties of BFO thin films, several recent attempts have been made, such as by substituting appropriate ion at either A-site, B-site or both sites of A and/or B [7–9]. It is reported that the co-substitution of double transition metal ions, or rare earth ions and transition metal ions, or alkaline earth metal ions and lanthanide rare earth ions can enhance the ferromagnetic and ferroelectric properties of BFO thin films [10–12].

Therefore, the co-substitution with four element ions of Mn, Cr, Sm and Sr could be an effective way to simultaneously improve the ferroelectric and magnetic properties of BFO thin films. So far, there have been fewer investigations on four elements co-substituted BFO thin films. In this work, Sr^{2+}-substituted $Bi_{0.89-x}Sm_{0.11}Sr_xFe_{0.94}(Mn_{0.04}Cr_{0.02})O_3$ (BSSrFMC, x=0.00, 0.02, 0.04 and 0.06) thin films were prepared on FTO/glass (SnO_2:F) substrates by using the sol–gel method. The effects of Sr^{2+}-substitution on the structure, leakage current, dielectric and multiferroic properties of BSSrFMC thin films were investigated systematically.

2. Experiments

Sr^{2+}-substituted $Bi_{0.89-x}Sm_{0.11}Sr_xFe_{0.94}(Mn_{0.04}Cr_{0.02})O_3$ thin films with x=0.00, 0.02, 0.04 and 0.06 were prepared on the FTO/glass substrates (FTO is the F-doped SnO_2

*Corresponding author. Tel.: +86 13759878391.
E-mail address: tan3114@163.com (G. Tan).

http://dx.doi.org/10.1016/j.ceramint.2014.05.032
0272-8842/

conductive film) by using the sol–gel method. The $BiFeO_3$ precursor solution was prepared using $Bi(NO_3)_3 \cdot 5H_2O$, $Sr(NO_3)_3$, $Sm(NO_3)_3 \cdot 5H_2O$, $Fe(NO_3)_3 \cdot 9H_2O$, $C_4H_6MnO_4 \cdot 4H_2O$ and $Cr(NO_3)_3 \cdot 9H_2O$ as raw materials, which were mixed together in an atomic ratio of $0.89-x$:x:0.11:0.94:0.04:0.02 (x=0, 0.02, 0.04, 0.06) (5 mol% of excess Bi was added to compensate for bismuth loss during the heat treatment). Then 2-methoxyethanol which served as a solvent was added into the raw materials and stirred for 1 h. Then acetic anhydride was added to dehydrate and adjust the pH value of the solution under constant stirring for 5 h (the volume ratio of 2-methoxyethanol and acetic anhydride was 3:1), and a stable precursor solution was obtained. The concentration of the solution was 0.3 mol/L. All the above processes were performed in an ambient atmosphere at room temperature. Meanwhile, the air humidity is less than 40%. FTO/glass substrates were washed in detergent, acetone, alcohol and deionized water sequentially. The precursor solution was spin coated on the FTO/glass substrates at 4000 rpm for 15 s with spin coating. After spin-coating, the wet films were dried at 240 °C for 5 min immediately to remove volatile materials and subsequently annealed at 550 °C for 10 min in the atmosphere for crystallization. Top Au electrodes of 0.502 mm^2 were deposited through a shadow mask on the surface of BFO films by sputtering. The films with top electrodes were annealed at 300 °C for 20 min for the electrode and the film to achieve full contact.

Japan Rigaku Company D/max-2200X-ray diffractometer (with Cu target, the scanning step length was 0.02° and operated at 40 kV, 20 mA) and laser Raman spectrometer (Horiba JYHR800 Raman system equipped with an Ar ion laser excitation at 534 nm) were used to identify the structure and crystallinity of the thin films; the surface morphologies of the thin films were observed by FE-SEM (Hitachi S4800); the chemical bonding states of the films were investigated by X-ray photoelectron spectroscopy (XPS, Kratos Ltd., XSAM 800). The electric hysteresis loops of the thin films were measured by an aix ACCT TF-Analyzer 2000. The leakage current of the thin films was measured by Agilent B2901A and the ferromagnetic properties of the thin films were tested by the MPMS-XL-7 superconducting quantum interference magnetic measuring system.

3. Results and discussion

Fig. 1(a) shows XRD patterns of $BSSr_xFMC$ thin films. An enlarged view of (110) peaks of the films is shown in Fig. 1(b). The main diffraction peaks of $BSSr_xFMC$ thin films were successfully indexed by using PDF card no. 20-0169. All the thin films are polycrystalline BFO phases with (110) preferential orientations. No impurity phase is detected in all the thin films. The FWHM values of the $BSSr_xFMC$ thin films are smaller than those of the non-doped BSFMC thin film, suggesting better crystallinities [13]. With increasing Sr^{2+} concentration, the (110) diffraction peaks are observed to shift towards lower 2θ value for $BSSr_xFMC$ thin films, indicating changes in lattice parameters due to relatively large ionic radius of Sr^{2+} ion (1.12 Å) compared with that of Bi^{3+} ion (1.03 Å) [14].

With regard to the better ferroelectric and ferromagnetic properties observed in the $BSSr_xFMC$ (x=0.04) thin film, the detailed structural analysis of the pure BFO and $BSSr_xFMC$ (x=0.00 and 0.04) thin films has been performed by Rietveld refinement [15,16] using "Maud" software [17,18]. Fig. 2(a)–(c) shows the observed, calculated and difference profiles of the studied specimens obtained after Rietveld refinements. The refinement result of the BFO thin film confirms a single trigonal phase, which belongs to R3c:H space group. However, the structure of the x=0.00 thin film was fitted very well to the tetragonal phase with P4 space group. In the case of the x=0.04 thin film, the contribution of the tetragonal phase with P4 space group is 95.34% and the tetragonal phase with P422 space group is 4.66%. This structural transformation will affect the multiferroic properties of the $BSSr_xFMC$ (x=0.04) thin film. With Sr^{2+}-substitution, the lattice constant a increases from 3.9415 to 3.9583 compared with the BSFMC thin film, resulting in unit cell volume expansion. This volume expansion can be expected because of the small difference between the ionic radius of Sr^{2+} (1.12 Å) ions and Bi^{3+} (1.03 Å) ions. Furthermore, the lattice parameters and schematics of the crystal structures of the thin films are also shown in Fig. 2.

The structural evolution of the $BSSr_xFMC$ thin films can also be expressed through Raman spectra. The Raman spectra of all thin films are shown in Fig. 3, which are fitted into individual Lorentzian components. According to the group theory, 13 Raman active modes ($4A_1+9E$) are predicted for the rhombohedrally distorted R3c space group for BFO [19]. For the pure BFO thin film, three peaks at 141.5, 169.7, and 214.9 cm^{-1} can be assigned to A_1 mode, and other peaks located at 262.0, 346.7, 467.2, 538.7 and 606.5 cm^{-1} are associated with E mode. However, three different aspects can be derived from the BSFMC thin film compared with the pure BFO. Firstly, the peak intensities decrease and increase for the A_1 and E-7 modes, respectively. Secondly, the A_1 and E modes greatly shift to higher frequencies. Thirdly, E-4 and E-6 modes disappear. This may be attributed to changes of Fe–O bonds with Sm-substitution at the Bi-site and (Mn, Cr) co-substitution at Fe site, which implies that a structural transition occurred in the BSFMC thin film. It shows shift of A_1 and E modes towards the high frequency side in the spectrum for $BSSr_xFMC$ thin films due to Sr^{2+}-substitution. Meanwhile, the peak intensity of E-7 mode increases with the increase of Sr^{2+} content. Changes in peak intensity and peak position demonstrate a small structural transition occurring in the $BSSr_xFMC$ thin films [20], which is consistent with the XRD data.

The FE-SEM micrographs of the $BSSr_xFMC$ thin films are shown in Fig. 4(a)–(d). It is observed that there are some pores in all the thin films. The grain size increases with increasing Sr^{2+}-substitution concentration. Greater grains are beneficial to achieving a good electrical property [21]. The values of grain sizes estimated from SEM records for x=0.00, x=0.02, x=0.04 and x=0.06 films are 20–40, 40–70, 50–80 and 50–90 nm, respectively. This result reveals that the Sr^{2+}-substitution is in favor of the grain growth of the $BSSr_xFMC$

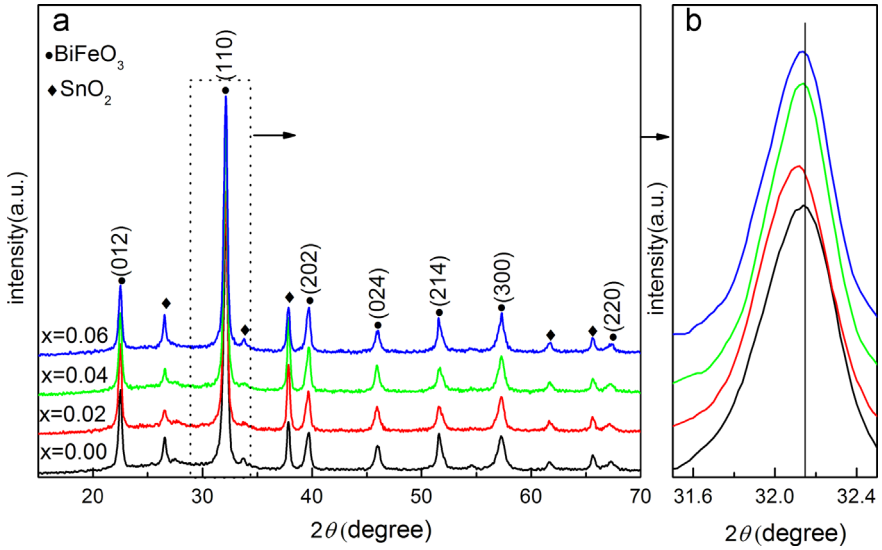

Fig. 1. (a) X-ray diffraction patterns of $BSSr_xFMC$ ($x=0.00$, 0.02, 0.04 and 0.06) thin films. (b) Enlarged view of (110) peaks of the films.

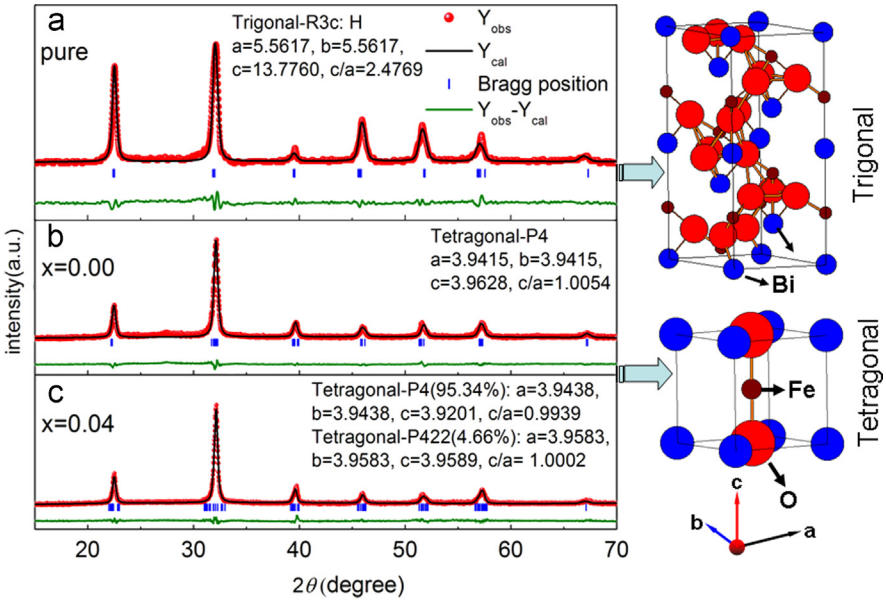

Fig. 2. Rietveld refinement of XRD patterns for pure BFO and $BSSr_xFMC$ ($x=0.00$, 0.04) thin films.

thin films. The interface between BFO and FTO is obvious and the thickness of BFO film is about 580 nm, as shown in Fig. 4(e).

To further investigate and validate the composition of the $BSSr_xFMC$ thin films with $x=0.02$, 0.04 and 0.06, the oxidation states of the Bi, Fe and O in the films were examined via XPS analysis at room temperature, as shown in Fig. 5. The peak positions and the corresponding peak areas are listed in Table 1. Fig. 5(a) shows the XPS survey spectra of the $BSSr_xFMC$ thin films with $x=0.02$, 0.04 and 0.06 in a wide energy range 0–1200 eV. It is clear from Fig. 5(a) that the Bi, Sm, Sr, Fe, Mn, Cr, O, and C elements are detected in the XPS spectrum, indicating that Bi, Sm, Sr, Fe, Mn and Cr ions in the films are in oxidation state. Fig. 5(b) shows that the Bi 4f doublets of the films consist of two main peaks, which are identified as Bi($4f_{7/2}$)–O and Bi($4f_{5/2}$)–O bonds, respectively [22]. It is evident from the doublet Bi $4f_{7/2}$, $4f_{5/2}$ lines that bismuth is in a single chemical state. Fig. 5(c) shows the coexistence of Fe $2p_{3/2}$ and $2p_{1/2}$ in the $BSSr_xFMC$ thin films with $x=0.02$, 0.04 and 0.06 which is confirmed by dividing the Fe $2p_{3/2}$ peak into two subpeaks. The concentration ratios of Fe^{3+} to Fe^{2+} ions are calculated to be 18.52:81.48, 17.85:82.15 and 10.31:89.69 for $x=0.02$, 0.04 and 0.06, respectively. Thus, Fe ion is in the mixed-valence state of Fe^{2+} and Fe^{3+} but Fe^{2+} state appears to be dominant for all the $BSSr_xFMC$ thin films, which is similar to the previous report [23–25]. The presence of Fe^{2+} ions means that oxygen vacancies meet electrical neutrality. Meanwhile, the oxygen vacancies act as a "bridge" between Fe^{3+} and Fe^{2+}, which significantly affects the electronic conduction and ferromagnetic

property of BFO [26]. Fig. 5(d) shows the XPS spectrum of O 1s. The result indicates that the concentration of oxygen vacancies in the $x=0.04$ film is the highest, followed by the $x=0.06$ film. This indicates that Sr^{2+}-substitution results in the increase of oxygen vacancy concentration due to the reaction $2Sr^{2+} \xrightarrow{2Bi^{3+}} 2Sr'_{Bi} + V''_O$ in the $BSSr_xFMC$ thin films.

Fig. 6 shows the leakage current density (J) vs. electric field (E) curves of the $BSSr_xFMC$ thin films which were measured at room temperature. It is found that the leakage current densities of the $BSSr_xFMC$ thin films decrease with the increase of Sr^{2+} content. At higher electric field (>450 kV/cm), the lowest leakage current is observed in the $x=0.04$ thin film. The leakage current density of the pure BFO thin film at 150 kV/cm is 10^{-3} A/cm^2. However, the leakage current densities of the $BSSr_xFMC$ thin films are all about 10^{-6} A/cm^2, which are 3 orders of magnitude lower than that of the BFO thin film. Moreover, as the applied electric field increases, the pure BFO and un-doped BSFMC thin film breakdown at 170 and 317 kV/cm, respectively. As for $BSSr_xFMC$ thin films, the breakdown field was improved to 630 kV/cm, which may be beneficial for possible applications in the high electric field.

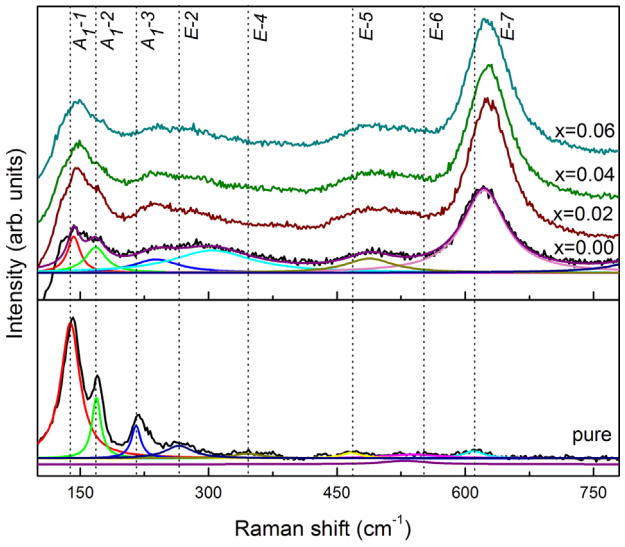

Fig. 3. Raman spectra of pure BFO and $BSSr_xFMC$ ($x=0.00$, 0.02, 0.04 and 0.06) thin films.

Fig. 7 shows the dielectric properties of the $BSSr_xFMC$ thin films that were measured at room temperature by varying the frequencies from 100 Hz to 1 MHz. It can be seen that the $BSSr_xFMC$ thin films show higher dielectric constant (ε_r) and higher dielectric loss ($\tan\delta$) than the pure BFO thin film. The highest ε_r value of 290 and relative low $\tan\delta$ value at 1 kHz are obtained in the $BSSr_xFMC$ thin film with $x=0.04$. This could be ascribed to the oxygen vacancies created by the substitution of Sr^{2+} for Bi^{3+} ions [27], and the oxygen vacancies can form defect dipoles with Sr'_{Bi}, such as $[2Sr'_{Bi}-V''_O]^x$, which may lead to increase of the $\tan\delta$ values of the $BSSr_xFMC$ thin films [28].

Fig. 8(a) shows the ferroelectric polarization (P) vs. electric field (E) curves of the pure BFO and $BSSr_xFMC$ thin films measured at 1 kHz. Compared with BFO and BSFMC thin films, the Sr^{2+}-substituted $BSSr_xFMC$ thin films shows effectively improved ferroelectric properties. The remanent polarization is

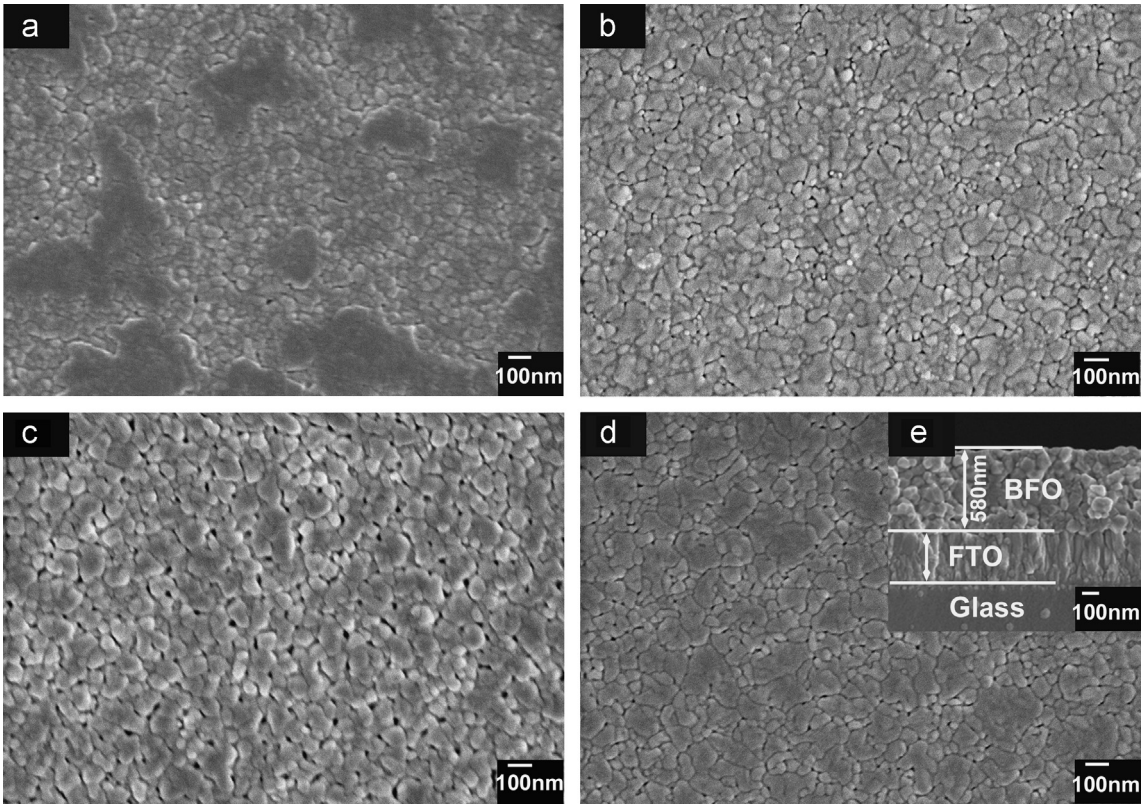

Fig. 4. FE-SEM surface-views of $BSSr_xFMC$ thin films for (a) $x=0.00$, (b) $x=0.02$, (c) $x=0.04$ and (d) $x=0.06$. (e) Cross-section views of $BSSr_xFMC$ thin films.

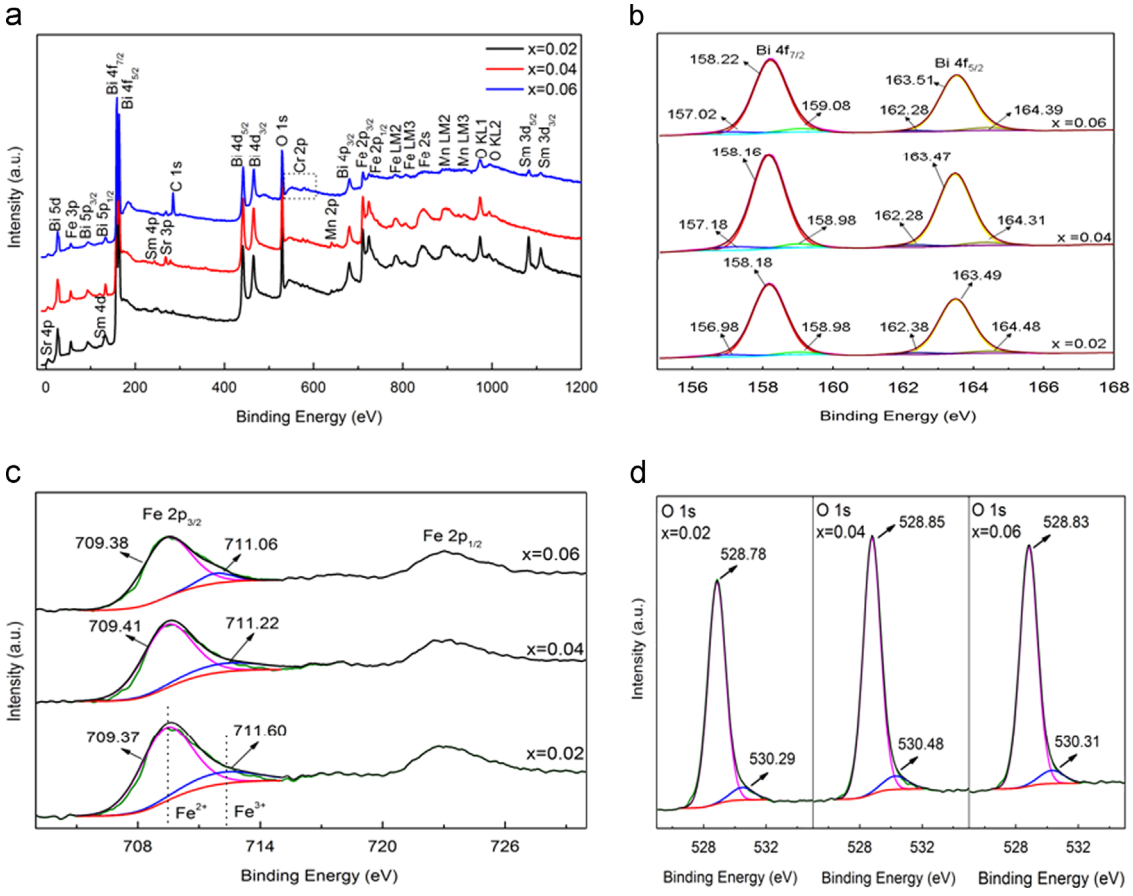

Fig. 5. (a) XPS survey spectra and high-resolution XPS spectra of (b) Bi 4f, (c) Fe 2p and (d) O 1s core levels of $x=0.02$, 0.04 and 0.06 thin films with the Gaussian dividing peak analysis.

Table 1
The binding energy of individual peak and corresponding peak area of Bi 4f, Fe $2p_{3/2}$ and O 1s core levels of the $BSSr_xFMC$ thin films with $x=0.02$, 0.04 and 0.06.

	Bi $4f_{7/2}$			Bi $4f_{5/2}$			Fe $2p_{3/2}$		O 1s	
$x=0.02$										
Position (eV)	158.18	156.98	158.98	163.49	162.38	164.48	709.37	711.60	528.78	530.29
Area (%)	45.28	2.53	2.16	46.27	2.77	0.99	81.48	18.52	93.02	6.98
$x=0.04$										
Position (eV)	158.16	157.18	158.98	163.47	162.28	164.31	709.41	711.22	528.85	530.48
Area (%)	45.71	1.80	2.49	46.05	2.20	1.75	82.15	17.85	93.19	6.81
$x=0.06$										
Position (eV)	158.22	157.02	159.08	163.51	162.28	164.39	709.38	711.06	528.83	530.31
Area (%)	45.94	1.80	2.26	45.70	2.44	1.86	89.69	10.31	92.87	7.13

increased with the increase of Sr^{2+} content, and the highest remanent polarization ($2P_r$) value of 173.43 μC/cm^2 is obtained in the $BSSr_xFMC$ ($x=0.04$) thin film at the maximum applied electric field of 727 kV/cm, as shown in Fig. 8(b). The remanent polarization values of the pure BFO and $BSSr_xFMC$ ($x=0.00$, 0.02, 0.04 and 0.06) thin films are 0.65, 54.29, 43.08, 86.88 and 71.87 μC/cm^2, respectively. Several reasons can be contributed to the enhanced polarization of the $BSSr_xFMC$ thin films. Firstly, the big remanent polarizations are attributed to a certain amount of disorder caused by Sr^{2+} ions [29]. Secondly, the greater grain size and the tetragonal phase can also be contributed to the enhancement of the ferroelectric properties [30]. Finally, the lower leakage current is another important factor. Fig. 8(c) shows the electric hysteresis loops and the polarization current curves of the $BSSr_xFMC$ ($x=0.04$) thin film measured at three frequencies: 500, 1000 and 2000 Hz. It is clear that the current mainly

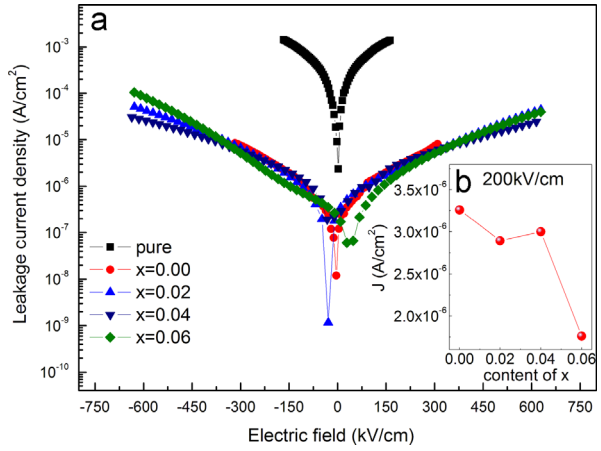

Fig. 6. Leakage current density (J) vs. electric field (E) of BSSr$_x$FMC (x=0.00, 0.02, 0.04 and 0.06) thin films measured at room temperature.

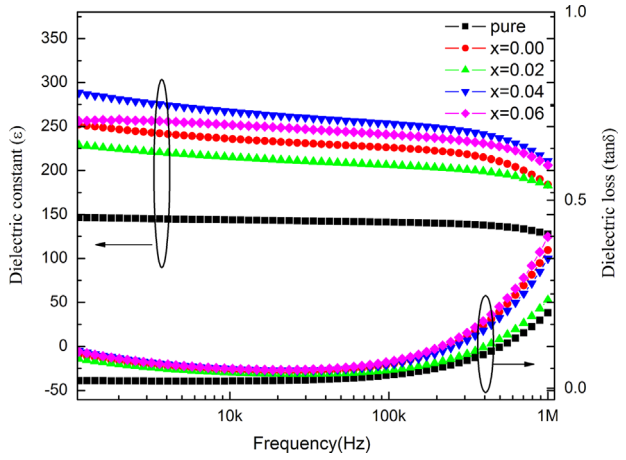

Fig. 7. Dielectric constant (ε_r) and dielectric loss (tanδ) of BSSr$_x$FMC (x=0.00, 0.02, 0.04 and 0.06) thin films measured at room temperature.

originates from the polarization reversal [31]. Around the coercive field (E_c), the rate of change of the polarization reaches its maximum and this leads to a sharp increase of the current density around E_c. It is obvious that the polarization current increases with the increase of frequency. The remanent polarization decreases and the coercive field increases with the increase of frequency at an applied electric field of 330 kV/cm, respectively.

The ferromagnetic properties of pure BFO and BSSr$_x$FMC thin films were measured under a low magnetic field of 8 kOe at room temperature as shown in Fig. 9. All the thin films exhibit typical M–H loops. Compared with BFO and BSFMC thin films, the ferromagnetism of the BSSr$_x$FMC thin films is effectively improved. With increase of Sr^{2+} content, the saturated magnetization (M_s) initially increases and then decreases, exhibiting a maximum value of 2.3 emu/cm^3 for BSSr$_x$FMC with x=0.04. The observed values of M_s for the pure BFO and BSSr$_x$FMC (x=0.00, 0.02, 0.04 and 0.06) thin films are 0.72, 1.2, 1.96, 2.3 and 1.90 emu/cm^3, respectively. The enhancement of ferromagnetism in BSSr$_x$FMC thin films can be ascribed to several reasons. Firstly, Sr^{2+}-substitution could further destroy the spiral modulated spin structure of

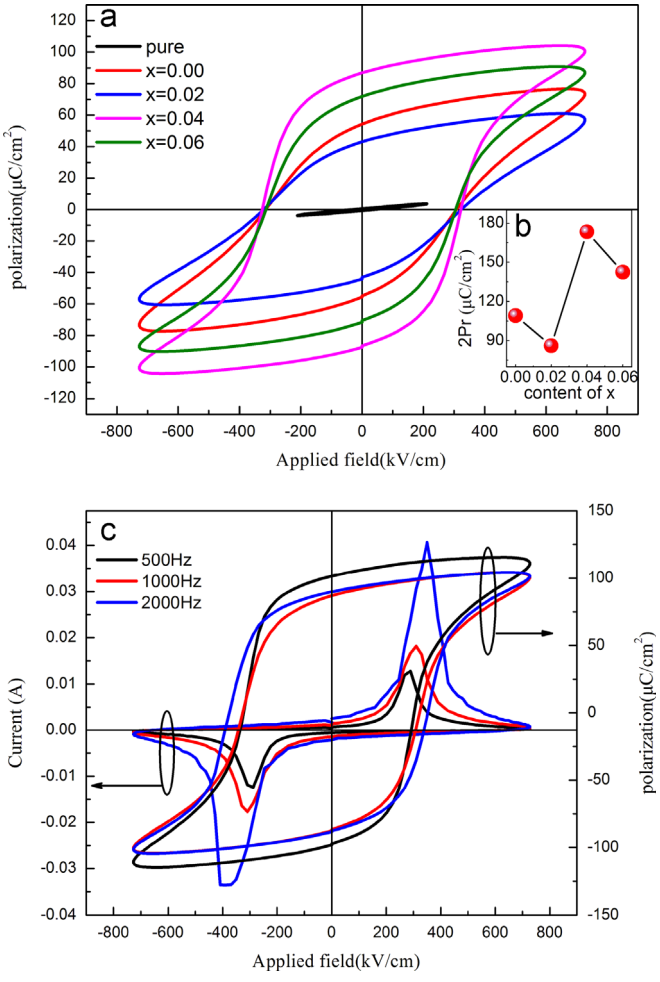

Fig. 8. (a) Electric hysteresis loops (P–E) of pure BFO and BSSr$_x$FMC (x=0.00, 0.02, 0.04 and 0.06) thin films. (b) 2P_r of films as a function of Sr-doping content increase. (c) Electric hysteresis loop of x=0.04 sample measured at three frequencies: 500, 1000 and 2000 Hz and the polarization current vs. applied electric field of x=0.04 sample for different frequencies.

$BiFeO_3$ [32]. Secondly, as Bi^{3+} ions were substituted by the low valence states of Sr^{2+} ions, the imbalance of charge would result in the existence of oxygen vacancies. The existence of oxygen vacancies is beneficial for the enhancement of the ferromagnetic properties [33]. Finally, with Sr^{2+}-substitution, the structure of BFO is further distorted and thus the bond angle of Fe–O–Fe should be changed, resulting in the enhancement of magnetization [34].

4. Conclusions

Sr^{2+}-substituted $Bi_{0.89-x}Sm_{0.11}Sr_xFe_{0.94}(Mn_{0.04}Cr_{0.02})O_3$ (BSSr$_x$FMC, x=0.00, 0.02, 0.04 and 0.06) thin films were prepared on FTO/glass (SnO_2:F) substrates by the sol–gel method annealed at 550 °C in atmosphere. The effects of Sr^{2+}-substitution on the structure, surface morphology, leakage current, dielectric and multiferroic properties of BSSrFMC thin films were investigated. The results show that the BSSr$_x$FMC thin film with x=0.04 exhibited the best multiferroic properties. Two crystal space groups coexist in thin film

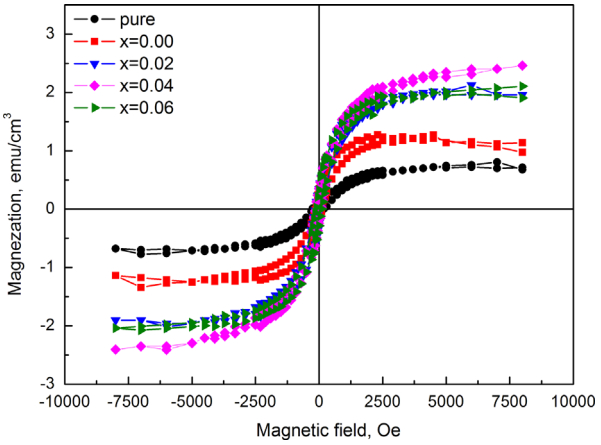

Fig. 9. Magnetic hysteresis loops (M–H) of the pure BFO and BSSr_xFMC (x=0.00, 0.02, 0.04 and 0.06) thin films measured at room temperature.

with x=0.04, which are tetragonal phase with P4 and P422 space groups. The ferroelectric and ferromagnetic properties of the BSFMC thin films have been successfully improved by alkali earth metal Sr^{2+}-substitution.

Acknowledgments

This work is supported by the Project of the National Natural Science Foundation of China (Grant no. 51372145); Research and Special Projects of the Education Department of Shaanxi Province (Grant no. 12JK0445); the Academic Leaders Funding Scheme of Shaanxi University of Science and Technology (2013XSD06); the Graduate Innovation Fund of Shaanxi University of Science and Technology (SUST-A04).

References

[1] Gustau Catalan, James F. Scott, Physics and applications of bismuth ferrite, Adv. Mater. 21 (2009) 2463.
[2] H. Uchida, Crystal structure and ferroelectric properties of rare-earth substituted $BiFeO_3$ thin films, J. Appl. Phys. 100 (2006) 014106.
[3] H.B. Yang, Y. Lin, M. Liu, J.F. Zhu, F. Wang, xBaTiO$_3$–(1 − x)BiFeO$_3$ strained epitaxial thin film with enhanced magnetization, Mater. Lett. 92 (2013) 427–429.
[4] X.Y. Mao, H. Sun, W. Wang, X.B. Chen, Y.L. Lu, Ferromagnetic, ferroelectric properties, and magneto-dielectric effect of $Bi_{4.25}La_{0.75}Fe_{0.5}Co_{0.5}Ti_3O_{15}$ ceramics, Appl. Phys. Lett. (2013) 072904.
[5] C.Y. Lan, Y.W. Jiang, S.G. Yang, Magnetic properties of La and (La, Zr) doped $BiFeO_3$ ceramics, J. Mater. Sci. 46 (2011) 734–738.
[6] C. Ederer, N.A. Spaldin, Weak ferromagnetism and magnetoelectric coupling in bismuth ferrite, Phys. Rev. B 71 (2005) 060401(R).
[7] Y. Wang, J. Li, J.Y. Chen, Y. Deng, Ba and Ti co-doped $BiFeO_3$ thin films via a modified chemical route with synchronous improvement in ferroelectric and magnetic behaviors, J. Appl. Phys. 113 (2013) 103904.
[8] J. Zhang, Y.J. Wu, X.K. Chen, X.J. Chen, Structural evolution and magnetization enhancement of $Bi_{1-x}Tb_xFeO_3$, J. Phys. Chem. Solids 74 (2013) 849–853.
[9] S.K. Singh, Structural and electrical properties of Sm-substituted $BiFeO_3$ thin films prepared by chemical solution deposition, Thin Solid Films 527 (2013) 126.
[10] A. Kumar, D. Varshney, Crystal structure refinement of $Bi_{1-x}Nd_xFeO_3$ multiferroic by the Rietveld method, Ceram. Int. 38 (2012) 3935–3942.
[11] K. Chakrabarti, K. Das, B. Sarkar, S. Ghosh, S.K. De, G. Sinha, J. Lahtinen, Enhanced magnetic and dielectric properties of Eu and Co co-doped $BiFeO_3$ nanoparticles, Appl. Phys. Lett. 101 (2012) 042401.
[12] J.Z. Huang, Y. Shen, M. Li, C.W. Nan, Structural transitions and enhanced ferroelectricity in Ca and Mn co-doped $BiFeO_3$ thin films, J. Appl. Phys. 110 (2011) 094106.
[13] B. Bhushan, A. Basumallick, N.Y. Vasanthacharya, S. Kumar, D. Das, Sr induced modification of structural, optical and magnetic properties in $Bi_{1-x}Sr_xFeO_3$ (x=0, 0.01, 0.03, 0.05 and 0.07) multiferroic nanoparticles, Solid. State. Sci. 12 (2010) 1063–1069.
[14] D. Varshney, A. Kumar, Structural, Raman and dielectric behavior in $Bi_{1-x}Sr_xFeO_3$ multiferroic, J. Mol. Struct. 1038 (2013) 242–249.
[15] W.J. Wu, D.Q. Xiao, J.G. Wu, W.F. Liang, J. Li, J.G. Zhu, Polymorphic phase transition-induced electrical behavior of $BiCoO_3$ modified $(K_{0.48}Na_{0.52})NbO_3$ lead-free piezoelectric ceramics, J. Alloys Compd. 509 (2011) L284–L288.
[16] H.E. Mgbemere, M. Hinterstein, G.A. Schneider, Structural phase transitions and electrical properties of $(K_xNa_{1-x})NbO_3$-based ceramics modified with Mn, J. Eur. Ceram. Soc. 32 (2012) 4341–4352.
[17] K. Chakrabarti, K. Das, B. Sarkar, S. Ghosh, S.K. De, G. Sinha, J. Lahtinen, Enhanced magnetic and dielectric properties of Eu and Co co-doped $BiFeO_3$ nanoparticles, Appl. Phys. Lett. 101 (2012) 042401.
[18] S. Chauhan, M. Kumar, S. Chhoker, S.C. Katyal, H. Singh, M. Jewariya, K.L. Yadav, Multiferroic, magnetoelectric and optical properties of Mn doped $BiFeO_3$ nanoparticles, Solid State Commun. 152 (2012) 525–529.
[19] C.M. Raghavan, J.W. Kim, S.S. Kim, Structural and ferroelectric properties of chemical solution deposited (Nd, Cu) co-doped $BiFeO_3$ thin film, Ceram. Int. 39 (2013) 3563–3568.
[20] Z.H. Duan, Q. Yu, J.D. Wu, J. Sun, Z.G. Hu, J.H. Chu, Lattice dynamics and dielectric functions of multiferroic $BiFeO_3$/c-sapphire films determined by infrared reflectance spectra and temperature-dependent Raman scattering, Thin Solid Films 525 (2012) 188–194.
[21] Y.J. Kim, J.W. Kim, C.M. Raghavan, J.J. Oak, H.J. Kim, W.J. Kim, M.H. Kim, T.K. Song, S.S. Kim, Enhancement of electrical properties of (Gd, V) co-doped $BiFeO_3$ thin films prepared by chemical solution deposition, Ceram. Int. 39 (2013) S195–S199.
[22] Z. Quan, W. Liu, H. Hu, et al., Microstructure, electrical and magnetic properties of Ce-doped $BiFeO_3$ thin films, J. Appl. Phys. 104 (2008) 084106.
[23] P.C. Juan, C.H. Wang, Electrical characterization of metal-ferroelectric (Mn-substituted $BiFeO_3$)-insulator (HfO_2)-semiconductor capacitors for nonvolatile memory applications, Microelectron. Eng. 86 (2009) 1845–1848.
[24] X. Xue, G.Q. Tan, G.H. Dong, W.L. Liu, H.J. Ren, Studies on structural, electrical and optical properties of multiferroic (Ag, Ni and In) codoped $Bi_{0.9}Nd_{0.1}FeO_3$ thin films, Appl. Surf. Sci. 292 (2014) 702–709.
[25] X. Xue, G.Q. Tan, W.L. Liu, H.J. Ren, Comparative study on multiferroic $(Bi_{0.9}RE_{0.1})(Fe_{0.97}Co_{0.03})O_{3-\delta}$(RE=Ce and Ho) thin films: structural, electrical and optical properties, Ceram. Int. 40 (2014) 6247–6254.
[26] S.J. Clark, J. Robertson, Energy levels of oxygen vacancies in $BiFeO_3$ by screened exchange, Appl. Phys. Lett. 94 (2009) 022902.
[27] H.L. Deng, M. Zhang, Q. Zhong, J.Z. Wei, H. Yan, Effect of Mn doping on multiferroic properties in $Bi_{0.8}Ba_{0.2}FeO_3$ ceramics, Ceram. Int. 40 (2014) 5869–5872.
[28] F. Yan, M.O. Lai, L. Lu, Enhanced multiferroic properties and valence effect of Ru-doped $BiFeO_3$ thin film, J. Phys. Chem. C 114 (2010) 6994–6998.
[29] F.X. Yan, G.Y. Zhao, N. Song, N.N. Zhao, Y.Q. Chen, In situ synthesis and characterization of fine-patterned La and Mn co-doped $BiFeO_3$ film, J. Alloys Compd. 570 (2013) 19–22.
[30] G.D. Hu, X. Cheng, W.B. Wu, C.H. Yang, Effects of Gd substitution on structure and ferroelectric properties of $BiFeO_3$ thin films prepared using metal organic decomposition, Appl. Phys. Lett. 91 (2007) 232909.
[31] G. Yu, X.F. Chen, F. Cao, G.H. Wang, X.L. Dong, Dynamic ferroelectric hysteresis scaling behavior of $40BiScO_3$–$60PbTiO_3$ bulk ceramics, Solid State Commun. 150 (2010) 1045–1047.

[32] X.L. Yu, X.Q. An, Enhanced magnetic and optical properties of pure and (Mn, Sr) doped $BiFeO_3$ nanocrystals, Solid State Commun. 149 (2009) 711–714.

[33] B. Wang, S.M. Wang, L.X. Gong, Z.F. Zhou, Structural, magnetic and photocatalytic properties of Sr^{2+}-doped $BiFeO_3$ nanoparticles based on an ultrasonic irradiation assisted self-combustion method, Ceram. Int. 38 (2012) 6643–6649.

[34] L.Y. Wang, D.H. Wang, H.B. Huang, Z.D. Han, Q.Q. Cao, B.X. Gu, Y.W. Du, The magnetic properties of polycrystalline $Bi_{1-x}Sr_xFeO_3$ ceramics, J. Alloys Compd. 469 (2009) 1–3.